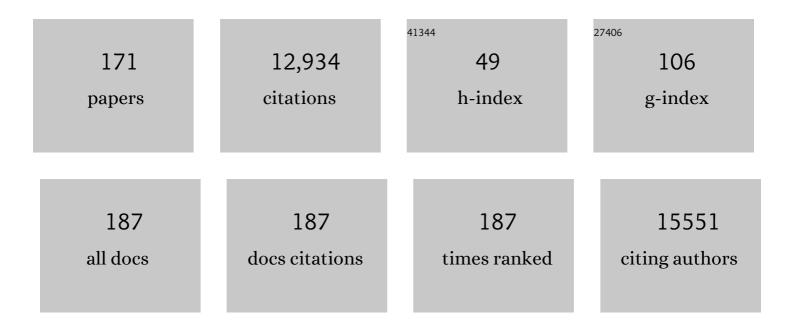
Oliver Speck

List of Publications by Year in descending order

Source: https://exaly.com/author-pdf/5276677/publications.pdf Version: 2024-02-01



#	Article	IF	CITATIONS
1	Neuroimaging standards for research into small vessel disease and its contribution to ageing and neurodegeneration. Lancet Neurology, The, 2013, 12, 822-838.	10.2	3,919
2	Point spread function mapping with parallel imaging techniques and high acceleration factors: Fast, robust, and flexible method for echo-planar imaging distortion correction. Magnetic Resonance in Medicine, 2004, 52, 1156-1166.	3.0	339
3	Magnetic resonance imaging of freely moving objects: prospective real-time motion correction using an external optical motion tracking system. NeuroImage, 2006, 31, 1038-1050.	4.2	339
4	Pros and cons of ultra-high-field MRI/MRS for human application. Progress in Nuclear Magnetic Resonance Spectroscopy, 2018, 109, 1-50.	7.5	331
5	Prospective motion correction in brain imaging: A review. Magnetic Resonance in Medicine, 2013, 69, 621-636.	3.0	320
6	Signalâ€ŧoâ€noise ratio and MR tissue parameters in human brain imaging at 3, 7, and 9.4 tesla using current receive coil arrays. Magnetic Resonance in Medicine, 2016, 75, 801-809.	3.0	299
7	Gender differences in the functional organization of the brain for working memory. NeuroReport, 2000, 11, 2581-2585.	1.2	258
8	Locus coeruleus imaging as a biomarker for noradrenergic dysfunction in neurodegenerative diseases. Brain, 2019, 142, 2558-2571.	7.6	219
9	Perfusion MRI and computerized cognitive test abnormalities in abstinent methamphetamine users. Psychiatry Research - Neuroimaging, 2002, 114, 65-79.	1.8	207
10	The impact of physiological noise correction on fMRI at 7 T. NeuroImage, 2011, 57, 101-112.	4.2	199
11	Vessel size imaging in humans. Magnetic Resonance in Medicine, 2005, 53, 553-563.	3.0	181
12	Measurement and Correction of Microscopic Head Motion during Magnetic Resonance Imaging of the Brain. PLoS ONE, 2012, 7, e48088.	2.5	177
13	Additive Effects of HIV and Chronic Methamphetamine Use on Brain Metabolite Abnormalities. American Journal of Psychiatry, 2005, 162, 361-369.	7.2	167
14	Perceptual Learning and Decision-Making in Human Medial Frontal Cortex. Neuron, 2011, 70, 549-559.	8.1	152
15	Response Properties of Human Amygdala Subregions: Evidence Based on Functional MRI Combined with Probabilistic Anatomical Maps. PLoS ONE, 2007, 2, e307.	2.5	144
16	1H-magnetic resonance spectroscopy in obsessive-compulsive disorder: evidence for neuronal loss in the cingulate gyrus and the right striatum. Psychiatry Research - Neuroimaging, 1997, 74, 173-176.	1.8	142
17	A high-resolution 7-Tesla fMRI dataset from complex natural stimulation with an audio movie. Scientific Data, 2014, 1, 140003.	5.3	139
18	Functional Imaging by IO- andT2* -parameter mapping using multi-image EPI. Magnetic Resonance in Medicine, 1998, 40, 243-248.	3.0	138

#	Article	IF	CITATIONS
19	Highest Resolution In Vivo Human Brain MRI Using Prospective Motion Correction. PLoS ONE, 2015, 10, e0133921.	2.5	138
20	Design and first baseline data of the DZNE multicenter observational study on predementia Alzheimer's disease (DELCODE). Alzheimer's Research and Therapy, 2018, 10, 15.	6.2	131
21	Robust and Fast Whole Brain Mapping of the RF Transmit Field B1 at 7T. PLoS ONE, 2012, 7, e32379.	2.5	127
22	Parallel imaging in non-bijective, curvilinear magnetic field gradients: a concept study. Magnetic Resonance Materials in Physics, Biology, and Medicine, 2008, 21, 5-14.	2.0	125
23	The molecular basis for gray and white matter contrast in phase imaging. NeuroImage, 2008, 40, 1561-1566.	4.2	115
24	Cortical thickness determination of the human brain using high resolution 3T and 7T MRI data. NeuroImage, 2013, 70, 122-131.	4.2	113
25	Blood Oxygen Level–Dependent MRI Allows Metabolic Description of Tissue at Risk in Acute Stroke Patients. Stroke, 2006, 37, 1778-1784.	2.0	108
26	High-Resolution MR Lymphangiography in Patients with Primary and Secondary Lymphedema. American Journal of Roentgenology, 2006, 187, 556-561.	2.2	99
27	Cerebral Blood Flow in a Healthy Circle of Willis and Two Intracranial Aneurysms: Computational Fluid Dynamics Versus Four-Dimensional Phase-Contrast Magnetic Resonance Imaging. Journal of Biomechanical Engineering, 2014, 136, .	1.3	95
28	Prospective Real-Time Slice-by-Slice Motion Correction for fMRI in Freely Moving Subjects. Magnetic Resonance Materials in Physics, Biology, and Medicine, 2006, 19, 55-61.	2.0	92
29	Laminar activity in the hippocampus and entorhinal cortex related to novelty and episodic encoding. Nature Communications, 2014, 5, 5547.	12.8	90
30	Perfusion MRI of the human brain with dynamic susceptibility contrast: Gradient-echo versus spin-echo techniques. Journal of Magnetic Resonance Imaging, 2000, 12, 381-387.	3.4	88
31	Functional magnetic resonance imaging: A review of methodological aspects and clinical applications. Journal of Magnetic Resonance Imaging, 2003, 18, 1-15.	3.4	87
32	High resolution single-shot EPI at 7T. Magnetic Resonance Materials in Physics, Biology, and Medicine, 2008, 21, 73-86.	2.0	87
33	Frontostriatal activation in patients with obsessive–compulsive disorder before and after cognitive behavioral therapy. Psychological Medicine, 2011, 41, 207-216.	4.5	86
34	Plasticity and Stability of the Visual System in Human Achiasma. Neuron, 2012, 75, 393-401.	8.1	85
35	A Rapid Sound-Action Association Effect in Human Insular Cortex. PLoS ONE, 2007, 2, e259.	2.5	85
36	Left frontal hub connectivity delays cognitive impairment in autosomal-dominant and sporadic Alzheimer's disease. Brain, 2018, 141, 1186-1200.	7.6	83

#	Article	IF	CITATIONS
37	Hippocampal vascular reserve associated with cognitive performance and hippocampal volume. Brain, 2020, 143, 622-634.	7.6	81
38	MR-Encephalography: Fast multi-channel monitoring of brain physiology with magnetic resonance. NeuroImage, 2007, 34, 212-219.	4.2	78
39	Enhancement of temporal resolution and BOLD sensitivity in real-time fMRI using multi-slab echo-volumar imaging. NeuroImage, 2012, 61, 115-130.	4.2	78
40	Systematic Regional Variations of GABA, Glutamine, and Glutamate Concentrations Follow Receptor Fingerprints of Human Cingulate Cortex. Journal of Neuroscience, 2013, 33, 12698-12704.	3.6	78
41	Anatomical specificity of functional amygdala imaging of responses to stimuli with positive and negative emotional valence. Journal of Neuroscience Methods, 2009, 180, 57-70.	2.5	74
42	SAR simulations for highâ€field MRI: How much detail, effort, and accuracy is needed?. Magnetic Resonance in Medicine, 2013, 69, 1157-1168.	3.0	72
43	Magnetic resonance imaging (MRI): A review of genetic damage investigations. Mutation Research - Reviews in Mutation Research, 2015, 764, 51-63.	5.5	72
44	Blood Oxygen Level–Dependent MRI of Cerebral CO ₂ Reactivity in Severe Carotid Stenosis and Occlusion. Stroke, 2005, 36, 751-756.	2.0	68
45	Higher CSF Tau Levels Are Related to Hippocampal Hyperactivity and Object Mnemonic Discrimination in Older Adults. Journal of Neuroscience, 2019, 39, 8788-8797.	3.6	64
46	High resolution fMRI of subcortical regions during visual erotic stimulation at 7 T. Magnetic Resonance Materials in Physics, Biology, and Medicine, 2008, 21, 103-111.	2.0	61
47	T1-weighted in vivo human whole brain MRI dataset with an ultrahigh isotropic resolution of 250 μm. Scientific Data, 2017, 4, 170032.	5.3	61
48	The BDNFVal66Met SNP modulates the association between beta-amyloid and hippocampal disconnection in Alzheimer's disease. Molecular Psychiatry, 2021, 26, 614-628.	7.9	61
49	A robust multi-scale approach to quantitative susceptibility mapping. NeuroImage, 2018, 183, 7-24.	4.2	60
50	Cerebral perfusion abnormalities in abstinent cocaine abusers: a perfusion MRI and SPECT study. Psychiatry Research - Neuroimaging, 2000, 99, 63-74.	1.8	58
51	Temporal Dynamics of Antidepressant Ketamine Effects on Glutamine Cycling Follow Regional Fingerprints of AMPA and NMDA Receptor Densities. Neuropsychopharmacology, 2017, 42, 1201-1209.	5.4	57
52	Dynamic magnetic resonance imaging of swallowing and laryngeal motion using parallel imaging at 3 T. Magnetic Resonance Imaging, 2009, 27, 48-54.	1.8	56
53	Highly accelerated PSF-mapping for EPI distortion correction with improved fidelity. Magnetic Resonance Materials in Physics, Biology, and Medicine, 2012, 25, 183-192.	2.0	56
54	High-resolution diffusion MRI at 7T using a three-dimensional multi-slab acquisition. NeuroImage, 2016, 143, 1-14.	4.2	55

#	Article	IF	CITATIONS
55	Retinotopic mapping of the human visual cortex at a magnetic field strength of 7T. Clinical Neurophysiology, 2009, 120, 108-116.	1.5	52
56	Singleâ€voxel MRS with prospective motion correction and retrospective frequency correction. NMR in Biomedicine, 2010, 23, 325-332.	2.8	51
57	Optimization of signal behavior in the transition to driven equilibrium in steady-state free precession sequences. Magnetic Resonance in Medicine, 2002, 48, 801-809.	3.0	50
58	Hippocampal vascularization patterns: A high-resolution 7 Tesla time-of-flight magnetic resonance angiography study. NeuroImage: Clinical, 2019, 21, 101609.	2.7	47
59	Functional spectroscopy of brain activation following a single light pulse: Examinations of the mechanism of the fast initial response. International Journal of Imaging Systems and Technology, 1995, 6, 203-208.	4.1	46
60	Navigator accuracy requirements for prospective motion correction. Magnetic Resonance in Medicine, 2010, 63, 162-170.	3.0	44
61	Fast31P chemical shift imaging using SSFP methods. Magnetic Resonance in Medicine, 2002, 48, 633-639.	3.0	42
62	Time Scales of Auditory Habituation in the Amygdala and Cerebral Cortex. Cerebral Cortex, 2010, 20, 2531-2539.	2.9	41
63	Default mode network connectivity change corresponds to ketamine's delayed glutamatergic effects. European Archives of Psychiatry and Clinical Neuroscience, 2020, 270, 207-216.	3.2	40
64	Systematic investigation of balanced steady-state free precession for functional MRI in the human visual cortex at 3 Tesla. Magnetic Resonance in Medicine, 2007, 57, 67-73.	3.0	39
65	Test–retest reliability of event-related functional MRI in a probabilistic reversal learning task. Psychiatry Research - Neuroimaging, 2009, 174, 40-46.	1.8	39
66	DNA double-strand breaks and micronuclei in human blood lymphocytes after repeated whole body exposures to 7T Magnetic Resonance Imaging. NeuroImage, 2016, 133, 288-293.	4.2	39
67	Prospective motion correction enables highest resolution timeâ€ofâ€flight angiography at 7T. Magnetic Resonance in Medicine, 2018, 80, 248-258.	3.0	39
68	Correlation of regional cerebral blood flow from perfusion MRI and SPECT in normal subjects. Magnetic Resonance Imaging, 1999, 17, 349-354.	1.8	37
69	Improved sensitivity to overlapping multiplet signals inin vivo proton spectroscopy using a multiecho volume selective (CPRESS) experiment. Magnetic Resonance in Medicine, 1997, 37, 816-820.	3.0	36
70	Reduced Cerebrovascular Reserve at CO2BOLD MR Imaging Is Associated with Increased Risk of Periinterventional Ischemic Lesions during Carotid Endarterectomy or Stent Placement: Preliminary Results1. Radiology, 2008, 249, 251-258.	7.3	36
71	Analysis of DNA Double-Strand Breaks and Cytotoxicity after 7 Tesla Magnetic Resonance Imaging of Isolated Human Lymphocytes. PLoS ONE, 2015, 10, e0132702.	2.5	36
72	Phase contrast imaging in neonates. NeuroImage, 2011, 55, 1068-1072.	4.2	35

#	Article	IF	CITATIONS
73	Effects of alternating current stimulation on the healthy and diseased brain. Frontiers in Neuroscience, 2015, 9, 391.	2.8	34
74	An improved PSF mapping method for EPI distortion correction in human brain at ultra high field (7T). Magnetic Resonance Materials in Physics, Biology, and Medicine, 2011, 24, 179-190.	2.0	33
75	Prospective motion correction improves highâ€resolution quantitative susceptibility mapping at 7T. Magnetic Resonance in Medicine, 2019, 81, 1605-1619.	3.0	33
76	Comparison of the hemodynamic response to different visual stimuli in single-event and block stimulation fMRI experiments. Journal of Magnetic Resonance Imaging, 2000, 12, 708-714.	3.4	32
77	High-resolution distortion-free diffusion imaging using hybrid spin-warp and echo-planar PSF-encoding approach. NeuroImage, 2017, 148, 20-30.	4.2	32
78	Advantages and Limitations of Prospective Head Motion Compensation for MRI Using an Optical Motion Tracking Device. Academic Radiology, 2006, 13, 1093-1103.	2.5	31
79	Automatic voxel positioning for MRS at 7ÂT. Magnetic Resonance Materials in Physics, Biology, and Medicine, 2015, 28, 259-270.	2.0	31
80	The traveling heads 2.0: Multicenter reproducibility of quantitative imaging methods at 7 Tesla. NeuroImage, 2021, 232, 117910.	4.2	31
81	Time-resolved measurements of brain activation after a short visual stimulus: new results on the physiological mechanisms of the cortical response. , 1997, 10, 222-229.		30
82	Separation and quantification of perfusion and BOLD effects by simultaneous acquisition of functionall0- andT*2-parameter maps. Magnetic Resonance in Medicine, 2001, 45, 811-816.	3.0	30
83	fMRI evidence for sensorimotor transformations in human cortex during smooth pursuit eye movements. Neuropsychologia, 2008, 46, 2203-2213.	1.6	30
84	Simultaneous correction for interscan patient motion and geometric distortions in echoplanar imaging. Magnetic Resonance in Medicine, 1999, 42, 201-205.	3.0	29
85	Visualization of the amygdalo–hippocampal border and its structural variability by 7T and 3T magnetic resonance imaging. Human Brain Mapping, 2014, 35, 4316-4329.	3.6	29
86	Fast chemical shift mapping with multiecho balanced SSFP. Magnetic Resonance Materials in Physics, Biology, and Medicine, 2006, 19, 267-273.	2.0	28
87	Impact of chiasma opticum malformations on the organization of the human ventral visual cortex. Human Brain Mapping, 2014, 35, 5093-5105.	3.6	28
88	Combined prospective and retrospective motion correction to relax navigator requirements. Magnetic Resonance in Medicine, 2011, 65, 1724-1732.	3.0	27
89	Distortion correction in EPI at ultraâ€highâ€field MRI using PSF mapping with optimal combination of shift detection dimension. Magnetic Resonance in Medicine, 2012, 68, 1239-1246.	3.0	27
90	Distortion Correction in EPI Using an Extended PSF Method with a Reversed Phase Gradient Approach. PLoS ONE, 2015, 10, e0116320.	2.5	26

#	Article	IF	CITATIONS
91	The traveling heads: multicenter brain imaging at 7 Tesla. Magnetic Resonance Materials in Physics, Biology, and Medicine, 2016, 29, 399-415.	2.0	26
92	CSF total tau levels are associated with hippocampal novelty irrespective of hippocampal volume. Alzheimer's and Dementia: Diagnosis, Assessment and Disease Monitoring, 2018, 10, 782-790.	2.4	26
93	Integration of ultra-high field MRI and histology for connectome based research of brain disorders. Frontiers in Neuroanatomy, 2013, 7, 31.	1.7	24
94	Impact of in Vivo High-Field-Strength and Ultra-High-Field-Strength MR Imaging on DNA Double-Strand-Break Formation in Human Lymphocytes. Radiology, 2017, 282, 782-789.	7.3	23
95	Prevention of motionâ€induced signal loss in diffusionâ€weighted echoâ€planar imaging by dynamic restoration of gradient moments. Magnetic Resonance in Medicine, 2014, 71, 2006-2013.	3.0	22
96	Correction of metal-induced susceptibility artifacts for functional MRI during deep brain stimulation. NeuroImage, 2017, 158, 26-36.	4.2	22
97	Imaging of the pial arterial vasculature of the human brain in vivo using high-resolution 7T time-of-flight angiography. ELife, 2022, 11, .	6.0	22
98	Sensory perceptions of individuals exposed to the static field of a 7T MRI: A controlled blinded study. Journal of Magnetic Resonance Imaging, 2015, 41, 1675-1681.	3.4	21
99	Transorbital alternating current stimulation modifies BOLD activity in healthy subjects and in a stroke patient with hemianopia: A 7 Tesla fMRI feasibility study. International Journal of Psychophysiology, 2020, 154, 80-92.	1.0	21
100	Comprehensive ultrahigh resolution whole brain in vivo MRI dataset as a human phantom. Scientific Data, 2021, 8, 138.	5.3	21
101	The effect of acquisition resolution on orientation decoding from V1 BOLD fMRI at 7 T. NeuroImage, 2017, 148, 64-76.	4.2	20
102	Transient flow prediction in an idealized aneurysm geometry using data assimilation. Computers in Biology and Medicine, 2019, 115, 103507.	7.0	20
103	Evidence for feature binding in the superior parietal lobule. NeuroImage, 2013, 68, 173-180.	4.2	19
104	The human habenula is responsive to changes in luminance and circadian rhythm. NeuroImage, 2019, 189, 581-588.	4.2	19
105	Fat navigators and Moiré phase tracking comparison for motion estimation and retrospective correction. Magnetic Resonance in Medicine, 2020, 83, 83-93.	3.0	19
106	Detection of Cerebral Microbleeds With Venous Connection at 7-Tesla MRI. Neurology, 2021, 96, e2048-e2057.	1,1	19
107	Correction of gradient nonlinearity artifacts in prospective motion correction for 7T MRI. Magnetic Resonance in Medicine, 2015, 73, 1562-1569.	3.0	18
108	Correction of B 0-induced geometric distortion variations in prospective motion correction for 7T MRI. Magnetic Resonance Materials in Physics, Biology, and Medicine, 2016, 29, 319-332.	2.0	18

#	Article	IF	CITATIONS
109	Motion Correction in Proton Resonance Frequency–based Thermometry in the Liver. Topics in Magnetic Resonance Imaging, 2018, 27, 53-61.	1.2	18
110	Optic Flow Stimuli in and Near the Visual Field Centre: A Group fMRI Study of Motion Sensitive Regions. PLoS ONE, 2008, 3, e4043.	2.5	17
111	GAD65 Promoter Polymorphism rs2236418 Modulates Harm Avoidance in Women via Inhibition/Excitation Balance in the Rostral ACC. Journal of Neuroscience, 2018, 38, 5067-5077.	3.6	17
112	European Ultrahighâ€Field Imaging Network for Neurodegenerative Diseases (EUFIND). Alzheimer's and Dementia: Diagnosis, Assessment and Disease Monitoring, 2019, 11, 538-549.	2.4	17
113	Perceived and mentally rotated contents are differentially represented in cortical depth of V1. Communications Biology, 2021, 4, 1069.	4.4	17
114	Amyloid pathology but not <i>APOE</i> ε4 status is permissive for tau-related hippocampal dysfunction. Brain, 2022, 145, 1473-1485.	7.6	17
115	Postoperative Lymphoceles: Detection with High-resolution MR Lymphangiography. Journal of Vascular and Interventional Radiology, 2006, 17, 1057-1062.	0.5	16
116	Variability of fMRIâ€response patterns at different spatial observation scales. Human Brain Mapping, 2012, 33, 1155-1171.	3.6	16
117	HIVâ€2 Infection With Cerebral Toxoplasmosis and Lymphomatoid Granulomatosis. Journal of Neuroimaging, 2001, 11, 212-216.	2.0	15
118	Visual motion, eye motion, and relative motion: A parametric fMRI study of functional specializations of smooth pursuit eye movement network areas. Journal of Vision, 2010, 10, 21-21.	0.3	15
119	Feasibility study: 7ÂT MRI in giant cell arteritis. Graefe's Archive for Clinical and Experimental Ophthalmology, 2016, 254, 1111-1116.	1.9	15
120	Motion correction of parametric fMRI data from multi-slice single-shot multi-echo acquisitions. Magnetic Resonance in Medicine, 2001, 46, 1023-1027.	3.0	14
121	Accurate quantification of water–macromolecule exchange induced frequency shift: Effects of reference substance. Magnetic Resonance in Medicine, 2013, 69, 263-268.	3.0	14
122	Efficacy of diphenhydramine in the prevention of vertigo and nausea at 7T MRI. European Journal of Radiology, 2013, 82, 768-772.	2.6	14
123	ReconResNet: Regularised residual learning for MR image reconstruction of Undersampled Cartesian and Radial data. Computers in Biology and Medicine, 2022, 143, 105321.	7.0	14
124	Comparison of static and dynamic MRI techniques for the measurement of regional cerebral blood volume. Magnetic Resonance in Medicine, 1999, 41, 1264-1268.	3.0	13
125	PSF mapping-based correction of eddy-current-induced distortions in diffusion-weighted echo-planar imaging. Magnetic Resonance in Medicine, 2016, 75, 2055-2063.	3.0	13
126	Modelâ€based iterative reconstruction for singleâ€shot <scp>EPI</scp> at 7 <scp>T</scp> . Magnetic Resonance in Medicine, 2017, 78, 2250-2264.	3.0	13

#	Article	IF	CITATIONS
127	Evaluation of exposure to (ultra) high static magnetic fields during activities around human MRI scanners. Magnetic Resonance Materials in Physics, Biology, and Medicine, 2017, 30, 255-264.	2.0	13
128	Prospective Head Motion Compensation for MRI by Updating the Gradients and Radio Frequency During Data Acquisition. Lecture Notes in Computer Science, 2005, 8, 482-489.	1.3	13
129	The European Federation of Organisations for Medical Physics Policy Statement No 14: The role of the Medical Physicist in the management of safety within the magnetic resonance imaging environment: EFOMP recommendations. Physica Medica, 2013, 29, 122-125.	0.7	12
130	False fMRI activation after motion correction. Human Brain Mapping, 2017, 38, 4497-4510.	3.6	12
131	Optimized EPI for fMRI using a slice-dependent template-based gradient compensation method to recover local susceptibility-induced signal loss. Magnetic Resonance Materials in Physics, Biology, and Medicine, 2010, 23, 165-176.	2.0	11
132	The separation of Cln and Clu in STEAM: a comparison study using short and long TEs/TMs at 3 and 7ÂT. Magnetic Resonance Materials in Physics, Biology, and Medicine, 2015, 28, 395-405.	2.0	11
133	Subjective perception of safety in healthy individuals working with 7ÂT MRI scanners: a retrospective multicenter survey. Magnetic Resonance Materials in Physics, Biology, and Medicine, 2016, 29, 379-387.	2.0	11
134	Assessment of Low-Grade Meniscal and Cartilage Damage of the Knee at 7 T. Investigative Radiology, 2018, 53, 390-396.	6.2	11
135	Neuronal glutamatergic changes and peripheral markers of cytoskeleton dynamics change synchronically 24 h after sub-anaesthetic dose of ketamine in healthy subjects. Behavioural Brain Research, 2019, 359, 312-319.	2.2	11
136	Hemodynamic Data Assimilation in aÂSubject-specific Circle of Willis Geometry. Clinical Neuroradiology, 2021, 31, 643-651.	1.9	11
137	Midbrain fMRI: Applications, Limitations and Challenges. Biological Magnetic Resonance, 2015, , 581-609.	0.4	11
138	Fast noniterative calibration of an external motion tracking device. Magnetic Resonance in Medicine, 2014, 71, 1489-1500.	3.0	10
139	Rostral Anterior Cingulate Glutamine/Glutamate Disbalance in Major Depressive Disorder Depends on Symptom Severity. Biological Psychiatry: Cognitive Neuroscience and Neuroimaging, 2019, 4, 1049-1058.	1.5	10
140	Triple visual hemifield maps in a case of optic chiasm hypoplasia. NeuroImage, 2020, 215, 116822.	4.2	10
141	Studying Alzheimer disease, Parkinson disease, and amyotrophic lateral sclerosis with 7-T magnetic resonance. European Radiology Experimental, 2021, 5, 36.	3.4	10
142	A new sequence for shaped voxel spectroscopy in the human brain using 2D spatially selective excitation and parallel transmission. NMR in Biomedicine, 2016, 29, 1028-1037.	2.8	8
143	Proton magnetic resonance spectroscopy in deep human brain structures at 7ÂT. Journal of Applied Spectroscopy, 2012, 79, 120-125.	0.7	7
144	The potential toxic impact of different gadolinium-based contrast agents combined with 7-T MRI on isolated human lymphocytes. European Radiology Experimental, 2018, 2, 40.	3.4	7

#	Article	IF	CITATIONS
145	The differential association between local neurotransmitter levels and wholeâ€brain restingâ€state functional connectivity in two distinct cingulate cortex subregions. Human Brain Mapping, 2022, 43, 2833-2844.	3.6	7
146	Chronic Lymphedema. Journal of Computer Assisted Tomography, 2006, 30, 688.	0.9	6
147	Quantitative assessment of visual cortex function with fMRI at 7 Tesla—test–retest variability. Frontiers in Human Neuroscience, 2015, 9, 477.	2.0	6
148	MRI and Genetic Damage: An Update. Current Radiology Reports, 2017, 5, 1.	1.4	6
149	Decoupling of the short-term hemodynamic response and the blood oxygen concentration. NMR in Biomedicine, 2001, 14, 402-407.	2.8	5
150	Percutaneous MR-guided interventions using an optical Moiré Phase tracking system: Initial results. PLoS ONE, 2018, 13, e0205394.	2.5	5
151	Phaseâ€Contrast MRI Detection of Ventricular Shunt CSF Flow: Proof of Principle. Journal of Neuroimaging, 2020, 30, 746-753.	2.0	5
152	Combined acquisition technique (CAT) for high-field neuroimaging with reduced RF power. Magnetic Resonance Materials in Physics, Biology, and Medicine, 2013, 26, 411-418.	2.0	4
153	Ultra high-field (7 T) multi-resolution fMRI data for orientation decoding in visual cortex. Data in Brief, 2017, 13, 219-222.	1.0	4
154	Noninvasive 4D Flow Characterization in a Stirred Tank via Phaseâ€Contrast Magnetic Resonance Imaging. Chemical Engineering and Technology, 2017, 40, 1370-1327.	1.5	4
155	Dissociable roles of cortical excitation-inhibition balance during patch-leaving versus value-guided decisions. Nature Communications, 2021, 12, 904.	12.8	4
156	Evaluation of 2D spatially selective MR spectroscopy using parallel excitation at 7 T. Quantitative Imaging in Medicine and Surgery, 2015, 5, 344-55.	2.0	4
157	Direct Magnetic Field Estimation Based on Echo Planar Raw Data. IEEE Transactions on Medical Imaging, 2010, 29, 1401-1411.	8.9	3
158	Quantitative evaluation of prospective motion correction in healthy subjects at 7T MRI. Magnetic Resonance in Medicine, 2022, 87, 646-657.	3.0	3
159	Assessment of measurement precision in singleâ€voxel spectroscopy at 7 T: Toward minimal detectable changes of metabolite concentrations in the human brain in vivo. Magnetic Resonance in Medicine, 2021, 87, 1119.	3.0	3
160	Chemical shift–based prospective kâ€space anonymization. Magnetic Resonance in Medicine, 2021, 85, 962-969.	3.0	2
161	Studying Alzheimer disease, Parkinson disease, and amyotrophic lateral sclerosis with 7-T magnetic resonance. European Radiology Experimental, 2021, 5, 36.	3.4	2
162	Rapid <scp>Geometryâ€Corrected Echoâ€Planar</scp> Diffusion ImagingÂat <scp>Ultrahigh</scp> Field: Fusing View Angle Tilting andÂ <scp>Pointâ€6pread</scp> Function Mapping. Magnetic Resonance in Medicine, 2022, 88, 2074-2087.	3.0	2

#	Article	IF	CITATIONS
163	Dynamic 2D selfâ€phaseâ€map Nyquist ghost correction for simultaneous multiâ€slice echo planar imaging. Magnetic Resonance in Medicine, 2018, 80, 1577-1587.	3.0	1
164	Wireless video transmission into the MRI magnet room: implementation and evaluation at 1.5T, 3T and 7T. Biomedizinische Technik, 2019, 64, 373-382.	0.8	1
165	Probabilistic Assignment of Brain Responses to the Human Amygdala and its Subregions using High Resolution Functional MRI. IFMBE Proceedings, 2009, , 807-810.	0.3	1
166	Perceived and mentally rotated contents are differentially represented in cortical layers of V1. Journal of Vision, 2020, 20, 766.	0.3	1
167	Contrasts, Mechanisms and Sequences. Medical Radiology, 2012, , 81-125.	0.1	0
168	Gain of Imaging Fidelity by Employing a Higher Number of Independent Transmit Channels Together with Slice-Selective Radio-Frequency (RF) Shimming at 7T. Materials, 2014, 7, 30-43.	2.9	0
169	Relative pressure field computation in human arteries based on 4D PC-MRI velocities. , 2014, , .		0
170	Improved Image Segmentation with Prospective Motion Correction in MRI. Informatik Aktuell, 2012, , 27-32.	0.6	0
171	3D-Printed Floating Cable Traps for MRI guided Microwave Ablation. , 2021, 2021, 1419-1422.		0